Simulating Astrophysical Jets in Laboratory Experiments

Paul M. Bellan, Setthivoine You, and Scott C. Hsu[†]
Caltech 128-95, Pasadena, CA 91125, USA

April 23, 1993

Abstract. Pulsed power technology and appropriate boundary conditions have been used to create simulations of magnetically driven astrophysical jets in a laboratory experiment. The experiments are quite reproducible and involve a distinct sequence. Eight initial flux tubes, corresponding to eight gas injection locations, merge to form the jet which lengthens, collimates, and eventually kinks. A model developed to explain the collimation process predicts that collimation is intimately related to convection and pile-up of frozen-in toroidal flux convected with the jet. The pile-up occurs when there is an axial non-uniformity in the jet velocity so that in the frame of the jet there appears to be a converging flow of plasma carrying frozen-in toroidal magnetic flux. The pile-up of convected flux at this "stagnation region" amplifies the toroidal magnetic field and increases the pinch force, thereby collimating the jet.

Keywords: astrophysical jet, collimation, kink, MHD, pinch, stagnation

1. Experiment motivation and design

A magnetically driven astrophysical jet is characterized by having a high Lundquist number and boundary conditions which typically consist of azimuthal symmetry, a mass source in the $z = 0$ plane and a poloidal magnetic field linking a rotating accretion disk in the $z = 0$ plane. Figure 1 sketches these boundary conditions and shows how the rotation of the accretion disk causes a radial electric field E_r which drives a poloidal current with associated toroidal magnetic field B_ϕ.

We have constructed an experimental configuration which simulates magnetically driven astrophysical jets. The experiment exploits technology previously developed for spheromaks, an MHD configuration relevant to magnetically confined controlled thermonuclear fusion research (Bellan, 2000). As shown in Fig. 2, the experimental boundary conditions are very similar to the astrophysical jet boundary conditions shown in Fig. 1. Rotating the annulus would provide an exact replica of the astrophysical jet boundary conditions, but the required rotation velocity would be impractically large. Instead of rotating the annulus, a high-energy capacitor bank is discharged across the gap separating the disk from the annulus. This alternative but equivalent way for producing the radial electric field E_r drives a current nearly along the poloidal

[†] now at LANL

field lines and similarly creates a toroidal magnetic field B_ϕ. Because MHD has no intrinsic scale, simulation of the dimensionless numbers and of the boundary conditions suffices to establish the conditions for creating a lab scale version of an astrophysical jet. The nominal parameters of the lab experiment are duration ~ 10 μs, $B \sim 0.01 - 0.1$ T, potential drop $\sim$1-6 kV, poloidal current $I \sim 50 - 150$ kA, density $n \sim 10^{19} - 10^{20}$ m^{-3}, typical $\beta << 1$, and Lundquist number $\sim 10^3$. Various types of gas species are used in order to observe the effect of changing the ion mass.

Figure 3 shows typical photographs in visible light (Hsu and Bellan, 2002) of a hydrogen plasma produced in these lab simulations of astrophysical jets. The central disk (20 cm diam) is surrounded by a co-planar, coaxial annulus (51 cm diam). Circular arrays of eight gas feed ports are located on both the disk and annulus; the disk is the cathode and the annulus, held at ground, is the anode. A magnetic field coil located just behind the disk provides a poloidal magnetic field simulating the field produced by a central object such as a star. There is a 6 mm gap insulating the disk from the annulus; high voltage is applied across this gap to drive the poloidal current between the disk and the annulus. The disk/annulus configuration is mounted on the end dome of a large cylindrical vacuum chamber the dimensions of which are so large (1.4 m diam, 2 m length) that there is ample room for the plasma to move without interacting with the walls. The large ratio of vacuum chamber dimensions to plasma dimensions thus approximates the unbounded space into which an actual astrophysical jet propagates.

The plasma evolves through a well-defined and reproducible sequence as follows:

1. Eight distinct, bright arched filamentary plasma loops form as shown in Fig. 3(top). These loops each span from a gas feed port on the cathode to a corresponding gas feed port on the anode. This configuration resembles the eight legs of a spider.

2. The portions of the 'spider legs' near the geometric axis (z-axis) merge to form a single central column as shown in Fig. 3 (second image from top) and the outer portions of the spider legs merge to form a mushroom-shaped return current. The central column constitutes the plasma jet.

3. The jet-like central column lengthens in the z direction as shown in Fig. 3 (third image from top). The cocoon-like return current also lengthens. The central column is very bright and collimated whereas the return current is dim and diffuse.

4. Upon reaching a critical length, the central column undergoes a kink instability (Hsu and Bellan, 2002; Hsu and Bellan, 2003) as shown in Fig. 3 (bottom image). The conditions for kink instability are in agreement with the Kruskal-Shafranov $q = 1$ instability condition for a cylindrical pinch where $q = 2\pi r B_\phi / B_z L$.

These results and the results from a related solar coronal loop simulation experiment have motivated a model (Bellan, 2003) for jet acceleration and collimation. This model shows that jet acceleration results from the non-conservative nature of the $\mathbf{J} \times \mathbf{B}$ MHD force and collimation results from compressibility of the jet and its embedded toroidal magnetic field. The model is discussed in detail in (Bellan, 2003) and a brief summary will now be given here.

The process is governed by ideal MHD and the relevant equations are the MHD equation of motion, the ideal MHD induction equation, and the equation of mass conservation, i.e.,

$$\rho \frac{d\mathbf{U}}{dt} = \mathbf{J} \times \mathbf{B} - \nabla P, \quad \frac{\partial \mathbf{B}}{\partial t} = \nabla \times (\mathbf{U} \times \mathbf{B}), \quad \frac{\partial \rho}{\partial t} = -\nabla \cdot (\rho \mathbf{U}). \quad (1)$$

The model is first worked out in a geometry simpler than an astrophysical jet but then extended to the astrophysical jet geometry. Cylindrical geometry $\{r, \phi, z\}$ is used and the term toroidal denotes the ϕ direction while the term poloidal denotes the r or z directions. The configuration is imagined to start as a finite-length, toroidally symmetric, current-free magnetic flux tube that is axially non-uniform as in Fig. 4 so that the initial magnetic field is purely poloidal and stronger at the two ends $z = \pm h$ than at the axial midpoint $z = 0$. The two flux tube ends intercept electrodes which can drive a current I along the flux tube (see green arrows in Fig.4). The decreased magnetic field strength at the axial midpoint means that the flux tube radius is larger at $z = 0$ than at $z = \pm h$. A bulged flux tube of this sort could be produced by two coaxial coils located at axial positions somewhat larger then $z = \pm h$. The dynamics is identified (Bellan, 2003) as consisting of three distinct stages.

The first stage, called the twisting stage, consists of the ramping up of the poloidal current I which is driven by an external electromotive force applied across the two end electrodes (this is topologically equivalent to the EMF applied across the disk and annulus electrodes in the astrophysical jet experiment). Because Ampere's law gives $B_\phi(r, z, t) = \mu_0 I(r, z, t)/2\pi r$ and because finite B_ϕ causes the flux tube to be twisted, the flux tube twists up in proportion to I. Thus, the twisting of the flux tube can be considered as being instantaneous upon the application of the current I. The amount of twisting is evaluated using the toroidal

component of the induction equation,

$$\frac{\partial B_\phi}{\partial t} = r\mathbf{B}_{pol}\cdot\nabla\left(\frac{U_\phi}{r}\right) - r\mathbf{U}_{pol}\cdot\nabla\left(\frac{B_\phi}{r}\right) - B_\phi\nabla\cdot\mathbf{U}_{pol}. \qquad (2)$$

The poloidal velocity $\mathbf{U}_{pol}$ is zero at this stage and also $\mathbf{B}_{pol}\cdot\nabla = B_{pol}\partial/\partial s$ where s is the distance along the flux tube from the $z=0$ midplane. By symmetry $U_\phi = 0$ on the $z=0$ plane, and so integrating Eq. (2) with respect to s and then invoking Ampere's law gives

$$U_\phi \approx \frac{\mu_0 s}{2\pi r B_{pol}}\frac{\partial I}{\partial t} \qquad (3)$$

which shows that a non-zero twist velocity requires a time-changing I.

The second stage occurs when the current has reached its steady-state value so that $\partial I/\partial t = 0$, but the system is not yet in dynamic equilibrium. In this stage, poloidal plasma flows (magenta arrows in Fig. 4) are accelerated by the $\mathbf{J}\times\mathbf{B}$ force (blue arrows in Fig.4). These flows are not instantaneous, but rather take time to develop. An approximate interpretation of these flows is to say that they are driven by axial gradients in the toroidal field energy $B_\phi^2/2\mu_0$. This is because the axial component of the $\mathbf{J}\times\mathbf{B}$ force can be expressed as $(\mathbf{J}\times\mathbf{B})_z = J_r B_\phi - J_\phi B_r$ and initially $J_\phi = 0$ because at initial times the flux tube retains its vacuum shape and J_ϕ is a function of the deviation of the flux tube from its vacuum shape. Using Ampere's law, the axial component of the $\mathbf{J}\times\mathbf{B}$ force is

$$(\mathbf{J}\times\mathbf{B})_z = -\frac{\partial}{\partial z}\left(\frac{B_\phi^2}{2\mu_0}\right) \qquad (4)$$

showing there exists an axial acceleration from regions where B_ϕ^2 is large to where it is small, i.e., from $z=\pm h$ towards $z=0$ because $B_\phi^2 = (\mu_0 I/2\pi r)^2$ is weaker at $z=0$ than at $z=\pm h$.

The third stage involves convergence of the flows at the axial midpoint $z=0$. The convergence at $z=0$ of the oppositely directed flows coming from the two endpoints leads to an axial compression of the plasma (shown as red in Fig. 4). Because the current is in steady state $U_\phi = 0$. At $z=0$ where $\mathbf{U}_{pol}=0$, Eq. (2) reduces to

$$\frac{\partial B_\phi}{\partial t} = -B_\phi\nabla\cdot\mathbf{U}_{pol}; \qquad (5)$$

this shows that flow convergence causes amplification of B_ϕ. Amplification occurs because compression of toroidal field lines frozen into the plasma, shown as red in Fig.4, occurs when the plasma itself becomes compressed; the plasma compression results as the oppositely directed flows collide at $z=0$. Because I is fixed, amplification of $B_\phi = \mu_0 I/2\pi r$

requires r to become smaller. Thus, the flow stagnation and resultant axial plasma compression causes the flux tube to become collimated.

These ideas can be generalized to the more complex geometry of an astrophysical jet by writing Eq. (2) as

$$\frac{d}{dt}\left(\frac{B_\phi}{r}\right) = \mathbf{B}_{pol}\cdot\nabla\left(\frac{U_\phi}{r}\right) - \frac{B_\phi}{r}\nabla\cdot\mathbf{U}_{pol}. \tag{6}$$

If the current I is constant in time, then there is no toroidal acceleration because toroidal acceleration requires existence of a current density normal to the poloidal flux surfaces. A steady current normal to flux surfaces is not possible because symmetry constrains the plasma particles to stay within a poloidal Larmor radius of a poloidal flux surface. This constrains any current normal to flux surfaces to be a transient AC current and consideration of microscopic particle motions shows that this current is the polarization current and is proportional to $\partial^2 I/\partial t^2$. Thus, if the plasma initially has $U_\phi = 0$, U_ϕ will revert to being zero when the current is in steady state. Equation (6) therefore reduces to

$$\frac{d}{dt}\left(\frac{B_\phi}{r}\right) = \quad -\frac{B_\phi}{r}\nabla\cdot\mathbf{U}_{pol} \tag{7}$$

which, after being combined with the continuity equation, becomes

$$\left(\frac{B_\phi}{r}\right)^{-1}\frac{d}{dt}\left(\frac{B_\phi}{r}\right) = \quad \frac{1}{\rho}\frac{d\rho}{dt}. \tag{8}$$

This shows that in the frame of the convecting plasma, B_ϕ increases in proportion to the compression of a fluid element. Hence, if an astrophysical jet has $\nabla\cdot\mathbf{U}_{pol} < 0$ then B_ϕ in convecting fluid elements will increase as these elements becomes axially squeezed. The increase in B_ϕ will cause the outer radius of the fluid elements to decrease because I is constant and $B_\phi = \mu_0 I/2\pi r$. Hence, any MHD poloidal flow with $\nabla\cdot\mathbf{U}_{pol} < 0$ and finite I will become collimated.

Acknowledgements

Supported by USDOE.

References

Bellan, P. M., *Spheromaks.* Imperial College Press, 2000.
Bellan, P. M., *Phys. Plasmas* 10 (5): 1999-2008 Part 2, 2003.
Hsu, S. C., and P. M. Bellan, *Mon. Not. Royal Astron. Soc.* 334 (2): 257-261, 2002.
Hsu, S. C., and P. M. Bellan, *Phys. Rev. Letters* 90 (21): art. no. 215002, 2003.

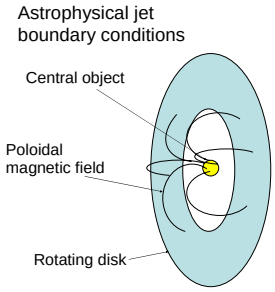

Figure 1. The accretion disk rotating with velocity U_ϕ cuts the poloidal magnetic field leading to a lab frame electric field $E_r = -U_\phi B_{pol}$. This radial electric field drives a poloidal current which flows in a direction approximately along the poloidal magnetic field and so generates a toroidal magnetic field B_ϕ.

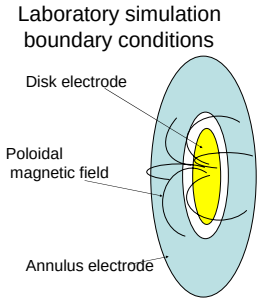

Figure 2. A capacitor bank connected between the central disk and the annulus creates a radial electric field E_r which drives current nearly along the poloidal field lines in analogy to the astrophysical situation.

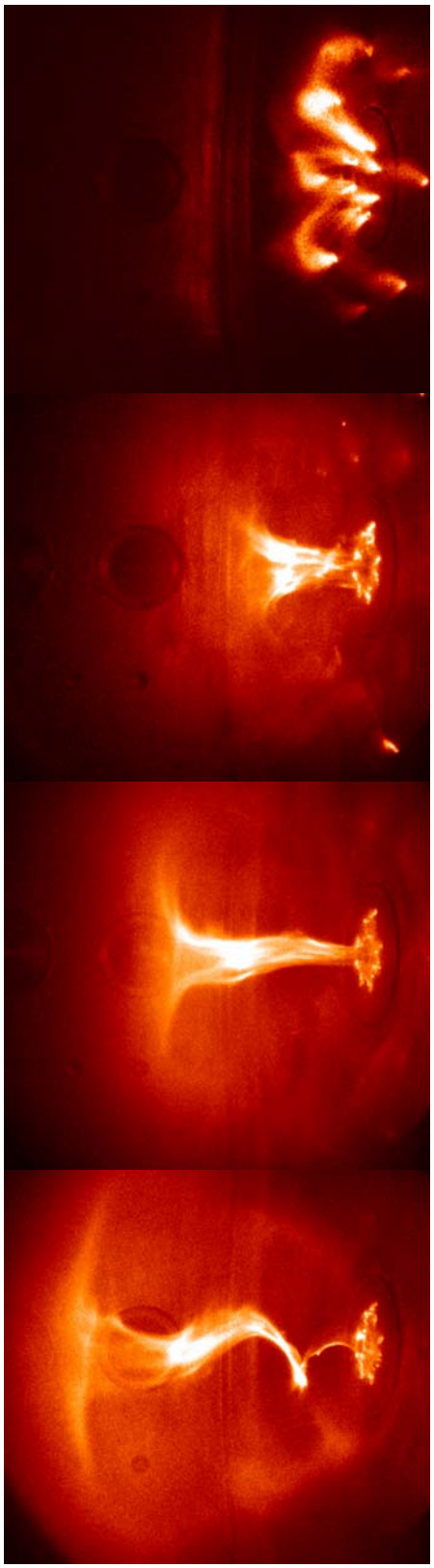

Figure 3. (on right) Photos showing experimental sequence from top to bottom: (i) eight plasma-filled loops form and span from gas ports on cathode to gas ports on cathode, (ii) the loops merge to form a central column jet, (iii) the jet lengthens and is collimated, (iv) the jet becomes kink unstable.

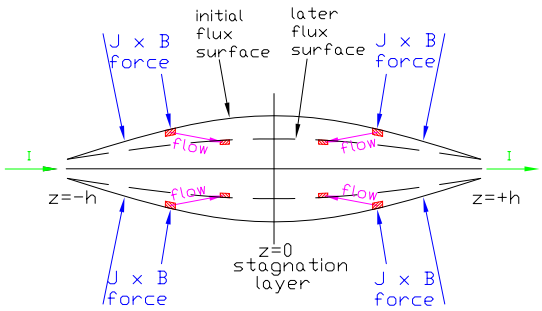

Figure 4. Sketch showing how convergence of flows from $z = \pm h$ towards $z = 0$ cause initially bulged flux tube to become collimated.